SUPPORTING INFORMATION

Modeling Nitric Oxide and its dimer: force field development and thermodynamics of dimerization

Tijin H.G. Saji,[†,‡] Thijs J.H. Vlugt,[¶] Sofia Calero,[†] and Behnaz Bagheri[*,†,‡]

†*Department of Applied Physics and Science Education, Technical University of Eindhoven, PO Box 513, 5600 MB, Eindhoven, The Netherlands*

‡*Institute for Complex Molecular Systems, PO Box 513, 5600 MB, Eindhoven, The Netherlands.*

¶*Process & Energy Department, Faculty of Mechanical, Maritime and Materials Engineering, Delft University of Technology, Leeghwaterstraat 39, 2628 CB, Delft, The Netherlands.*

E-mail: b.bagheri@tue.nl

Table S1: Experimental values for structural properties of NO and $(NO)_2$.[1,2]

Structural properties	Experimental[1,2]
NO	
r(NO)/Å	1.151
$(NO)_2$	
r(NN)/Å	2.263
r(NO)/Å	1.152
∠ ONO/°	97.120

Table S2: Experimental vibrational frequencies of NO and $(NO)_2$.[2–4]

Vibrational frequencies/[cm^{-1}]	Experimental[2–4]
NO	
ν_1	1904.2
$(NO)_2$	
ν_1	1868
ν_2	239
ν_3	135
ν_4	117
ν_5	1789
ν_6	429

Table S3: Experimental rotational constants of NO and $(NO)_2$.[5]

Rotational constants/[cm^{-1}]	Experimental[5]
NO	
B	1.67195
$(NO)_2$	
A	0.86159
B	0.18728
C	0.15363

Table S4: $\ln(\frac{qV_0}{\Lambda^3})$ of NO and $(NO)_2$ as a function of temperature.

Temperature /[K]	$\ln(\frac{qV_0}{\Lambda^3})_{NO}$/[-]	$\ln(\frac{qV_0}{\Lambda^3})_{(NO)_2}$/[-]
121.5	631.82	1270.67
125	614.44	1235.59
130	591.23	1188.80
135	569.75	1145.50
140	549.79	1105.25
145	531.23	1067.84
150	513.89	1032.86
155	497.68	1000.20
160	482.49	969.55
165	468.19	940.76

Table S5: Coexistence densities of the reactive NO-$(NO)_2$ system as a function of temperature, computed using the New FF (see Table II of the main manuscript). Experimental liquid densities[6] are listed for comparison. The subscripts show the standard deviations computed from the results of the 5 independent production runs.

Temperature /[K]	ρ_{gas} /[kg/m^3]	ρ_{liquid} /[kg/m^3]	$\rho_{liquid\text{-}Expt.}$ /[kg/m^3]
121.5	$3.31_{0.1}$	$1280.30_{1.0}$	1280.27
125	$4.61_{0.1}$	$1263.04_{0.8}$	1263.23
130	$7.04_{0.2}$	$1236.86_{0.6}$	1237.83
135	$10.84_{0.1}$	$1208.25_{0.9}$	1211.01
140	$15.40_{0.1}$	$1179.97_{1.0}$	1182.50
145	$22.01_{0.4}$	$1147.75_{0.7}$	1151.92
150	$29.36_{0.5}$	$1114.70_{1.4}$	1118.78
155	$39.22_{0.6}$	$1076.79_{0.7}$	1082.32
160	$54.20_{0.6}$	$1039.23_{1.5}$	1041.36
165	$69.85_{1.2}$	$994.66_{0.4}$	993.86

Table S6: $(NO)_2$ mole fractions (χ) in gas and liquid of the reactive NO-$(NO)_2$ system as a function of temperature, computed using the New FF (see Table II of the main manuscript). The errors are within 1% of the reported values. Experimental $(NO)_2$ mole fractions[7,8] are listed for comparison.

Temperature /[K]	$\chi_{(NO)_2\,\text{gas}}$	$\chi_{(NO)_2\,\text{liquid}}$	$\chi_{(NO)_2\,\text{liquid-Expt.}}$
110	0.05	0.92	0.95
115	0.06	0.89	—
121.5	0.06	0.86	—
125	0.06	0.83	—
130	0.07	0.80	0.85
135	0.07	0.75	—
140	0.07	0.72	0.76
145	0.07	0.67	—
150	0.08	0.63	0.65
155	0.08	0.58	—
160	0.08	0.53	0.53
165	0.08	0.48	—

a Experimental data for 110 K and 115 K are obtained from Smith and Johnston.[7] Data from 121.5 K to 165 K are extrapolated values obtained from Refs.[8,9] using the WebPlotDigitizer tool.[10]

Table S7: Saturated vapor pressures of the reactive NO-$(NO)_2$ system computed using the New FF (see Table II of the main manuscript). The standard deviations are given as subscripts. Experimental values[6] are listed for comparison.

Temperature /[K]	P_{sat} /[MPa]	$P_{\text{sat-Expt.}}$ /[MPa]
121.5	$0.09_{0.01}$	0.10
125	$0.13_{0.01}$	—
130	$0.22_{0.009}$	0.26
135	$0.35_{0.02}$	—
140	$0.54_{0.02}$	0.59
145	$0.79_{0.02}$	—
150	$1.12_{0.01}$	1.35
155	$1.51_{0.02}$	—
160	$2.00_{0.03}$	2.60
165	$2.65_{0.04}$	—

Table S8: Average number of NO (N_{NO}) and $(\mathrm{NO})_2$ ($N_{(\mathrm{NO})_2}$) molecules and volumes (V) in the vapor and liquid simulation boxes of the reactive NO-$(\mathrm{NO})_2$ system computed at different temperatures using the New FF. The standard deviations are given in subscripts.

T/[K]	$N_{\mathrm{NO,\ liquid}}$	$N_{(\mathrm{NO})_2,\ \mathrm{liquid}}$	$N_{\mathrm{NO,\ vapor}}$	$N_{(\mathrm{NO})_2,\ \mathrm{vapor}}$	$V_{\mathrm{liquid}}/[\mathrm{Å}^3]$	$V_{\mathrm{vapor}}/[\mathrm{Å}^3]$
121.5	$55.45_{2.06}$	$334.22_{1.09}$	$3.63_{0.13}$	$0.23_{0.02}$	$28264.32_{18.11}$	$63408.19_{18.11}$
125	$65.46_{1.40}$	$328.39_{0.78}$	$5.08_{0.14}$	$0.34_{0.02}$	$28589.98_{15.12}$	$63082.53_{15.12}$
130	$81.94_{1.44}$	$318.65_{0.83}$	$7.68_{0.24}$	$0.54_{0.03}$	$29083.53_{9.93}$	$62588.99_{9.93}$
135	$93.68_{1.33}$	$288.40_{0.70}$	$3.93_{0.08}$	$0.30_{0.01}$	$27754.99_{18.07}$	$21093.83_{18.07}$
140	$109.74_{1.39}$	$279.54_{0.74}$	$5.36_{0.09}$	$0.41_{0.02}$	$28349.38_{21.06}$	$20499.44_{21.06}$
145	$131.40_{0.92}$	$267.52_{0.54}$	$7.36_{0.13}$	$0.59_{0.02}$	$29042.59_{9.64}$	$19806.23_{9.64}$
150	$150.61_{1.85}$	$254.79_{0.93}$	$12.76_{0.11}$	$1.03_{0.02}$	$29628.99_{34.76}$	$25739.07_{34.76}$
155	$168.89_{0.67}$	$230.92_{0.41}$	$20.81_{0.30}$	$1.73_{0.05}$	$29296.78_{26.28}$	$31259.44_{26.28}$
160	$201.24_{1.45}$	$227.70_{0.78}$	$15.58_{0.23}$	$1.39_{0.03}$	$31614.61_{30.47}$	$17234.21_{30.47}$
165	$241.49_{0.86}$	$223.31_{0.61}$	$26.96_{0.33}$	$2.46_{0.06}$	$34580.31_{12.93}$	$23010.43_{12.93}$

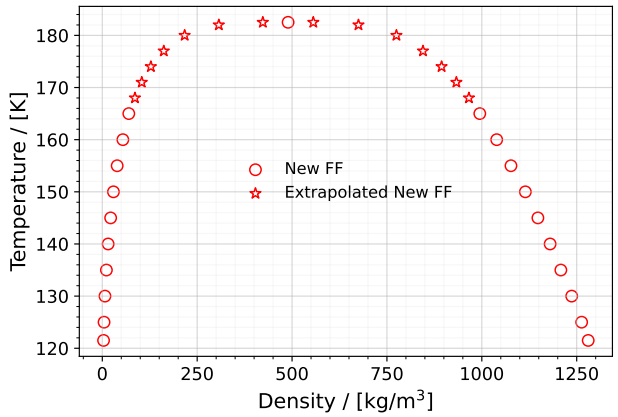

Figure S1: Vapor-liquid coexistence densities of the reactive NO-$(\mathrm{NO})_2$ system predicted using the New FF as a function of temperature (red circles). The extrapolated vapor-liquid coexistence densities obtained by fitting the liquid and vapor phase densities to the law of rectilinear diameters are also shown (red stars).

Table S9: Force field parameters developed for the NO molecule by Zhou *et al.*[11] (Zhou FF) and Lachet *et al.*[12] (Lachet FF).

	Species	ϵ/[K]	σ/[Å]	$q/[e]$
Zhou FF	N	79.50	3.014	0.0288
	O	96.94	2.875	−0.0288
Lachet FF	NO	130.00	3.40	–

Table S10: Critical temperature (T_c), density (ρ_c), and pressure (P_c) for pure NO and pure $(NO)_2$ computed using our newly developed force field (New FF) as well as the force fields developed by Zhou *et al.*[11] and Lachet *et al.*[12]

NO	T_c/[K]	ρ_c/[kg/m^3]	P_c/[MPa]
New FF	167.34	414.82	5.49
Zhou FF	277.15	427.23	8.66
Lachet FF	168.20	400.27	5.31

$(NO)_2$	T_c/[K]	ρ_c/[kg/m^3]	P_c/[MPa]
New FF	243.78	454.28	4.51
Lachet FF	298.37	449.95	5.31

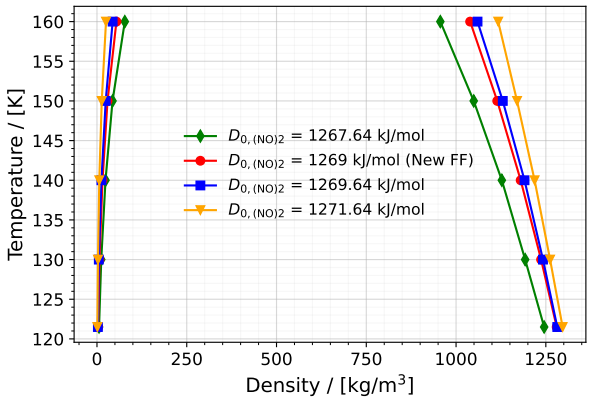

Figure S2: Vapor-liquid coexistence densities of the reactive NO-$(NO)_2$ system for various values of $D_{0,(NO)_2}$ using the New FF.

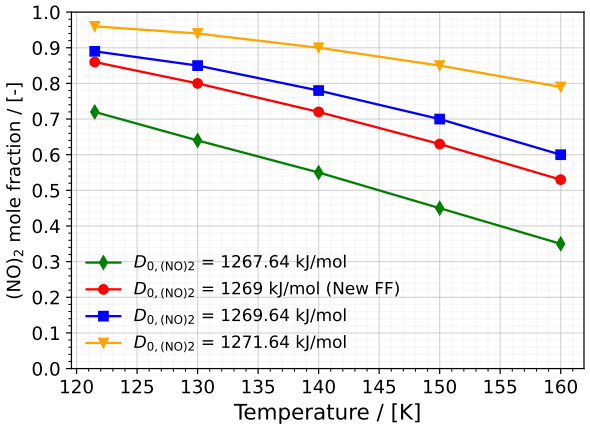

Figure S3: Dimer mole fractions in the liquid phase of the reactive NO-$(NO)_2$ system for various values of $D_{0,(NO)_2}$ using the New FF.

Table S11: Critical temperature (T_c) and density (ρ_c) for various values of $D_{0,(NO)_2}$ which were used to study the sensitivity of the VLE properties of the reactive NO-$(NO)_2$ system to the atomization energy of $(NO)_2$. L-J parameters and partial charges are taken from the New FF. $D_{0,(NO)_2} = 1268\,\mathrm{kJ/mol}$ is the value with which the VLE properties can be obtained in excellent agreement with experiments.

$D_{0,(NO)_2}$/[kJ/mol]	T_c/[K]	ρ_c/[kg/m^3]
1267.64	175.94	472.85
1269	182.51	489.59
1269.64	182.26	500.81
1271.64	194.94	500.83

Table S12: List of the force field parameters used to study the sensitivity of VLE properties to the L-J parameters, σ and ϵ, of NO and/or $(NO)_2$. The New FF is also included for comparison. In each combination, the L-J parameters of NO and/or $(NO)_2$ are varied by $\pm 10\%$ compared to the respective parameters of the New FF. The differences of each combination compared to the New FF is shown in bold. ϵ/k_B is in units of Kelvin and σ is in units of Å.

	$\frac{\epsilon}{k_B}$N-N_2O_2	$\sigma_{N\text{-}N_2O_2}$	$\frac{\epsilon}{k_B}$O-N_2O_2	$\sigma_{O\text{-}N_2O_2}$	$\frac{\epsilon}{k_B}$N-NO	$\sigma_{N\text{-}NO}$	$\frac{\epsilon}{k_B}$O-NO	$\sigma_{O\text{-}NO}$
FF-a	47.00	**2.72**	54.52	**2.58**	48.50	3.09	56.29	2.94
FF-b	47.00	**3.32**	54.52	**3.16**	48.50	3.09	56.29	2.94
FF-c	**42.30**	3.02	**49.07**	2.87	48.50	3.09	56.29	2.94
FF-d	**51.70**	3.02	**59.97**	2.87	48.50	3.09	56.29	2.94
FF-e	47.00	3.02	54.52	2.87	48.50	**2.78**	56.29	**2.65**
FF-f	47.00	3.02	54.52	2.87	48.50	**3.40**	56.29	**3.23**
FF-g	47.00	3.02	54.52	2.87	**43.65**	3.09	**50.66**	2.94
FF-h	47.00	3.02	54.52	2.87	**53.35**	3.09	**61.92**	2.94
FF-i	47.00	**2.72**	54.52	**2.58**	48.50	**2.78**	56.29	**2.65**
FF-j	47.00	**3.32**	54.52	**3.16**	48.50	**3.40**	56.29	**3.23**
FF-k	**42.30**	3.02	**49.07**	2.87	**43.65**	3.09	**50.66**	2.94
FF-l	**51.70**	3.02	**59.97**	2.87	**53.35**	3.09	**61.92**	2.94
New FF	47.00	3.02	54.52	2.87	48.50	3.09	56.29	2.94

Table S13: Critical temperatures (T_c) and densities (ρ_c) for the force field parameters listed in Table S11, which were used to study the sensitivity of the VLE properties on σ and ϵ parameters.

	T_c/[K]	ρ_c/[kg/m^3]
FF-a	177.90	460.42
FF-b	189.86	463.39
FF-c	178.57	452.20
FF-d	190.54	523.43
FF-e	182.68	562.30
FF-f	184.56	368.04
FF-g	178.91	519.04
FF-h	190.60	447.92
FF-i	176.85	597.30
FF-j	188.48	406.17
FF-k	173.47	484.92
FF-l	189.97	495.64
New FF	182.51	489.59

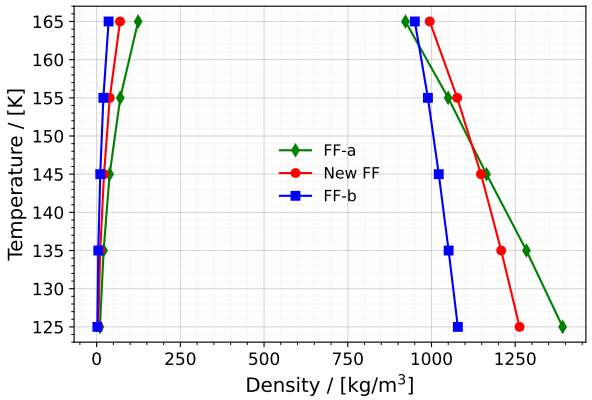

Figure S4: Orthobaric coexistence densities of the reactive NO-$(NO)_2$ system using FF-a (green diamonds), the New FF (blue circles), and FF-b (red squares).

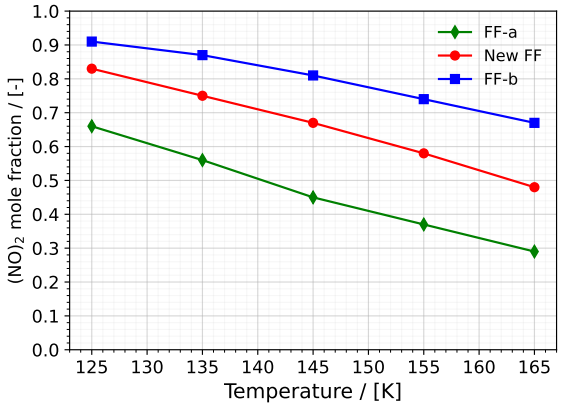

Figure S5: $(NO)_2$ mole fractions in the liquid phase of the reactive NO-$(NO)_2$ system using FF-a (green diamonds), the New FF (blue circles), and FF-b (red squares).

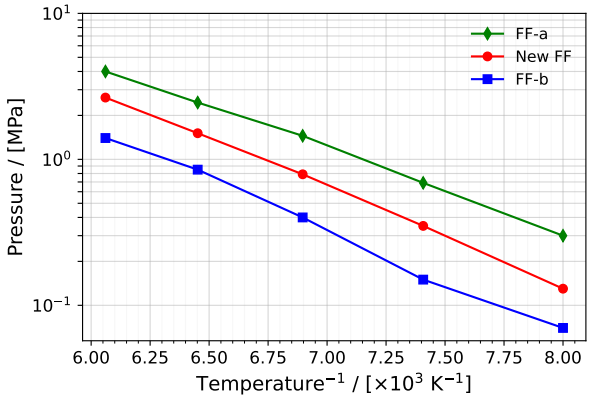

Figure S6: Inverse temperature dependence of the saturated vapor pressures of the reactive NO-$(NO)_2$ system using FF-a (green diamonds), the New FF (blue circles), and FF-b (red squares), in logarithmic scale.

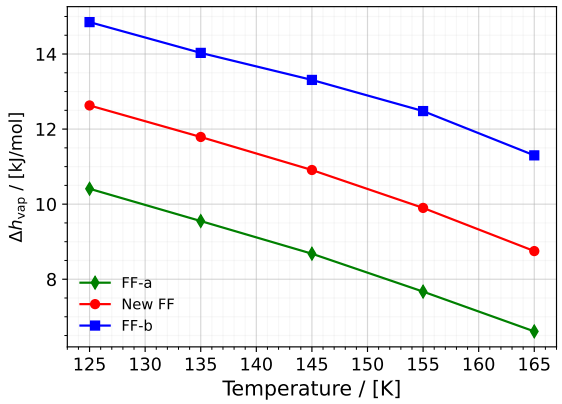

Figure S7: Heats of vaporization of the reactive NO-$(NO)_2$ system using FF-a (green diamonds), the New FF (blue circles), and FF-b (red squares).

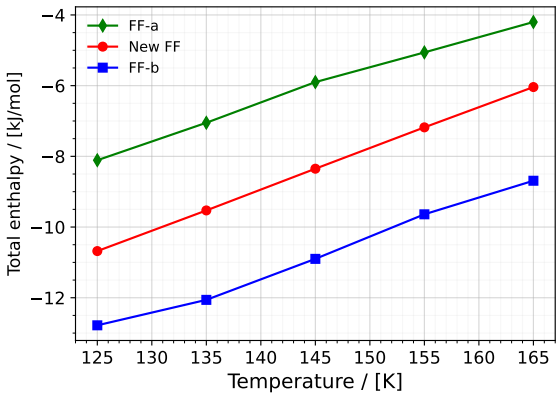

Figure S8: Total true molar enthalpies of the reactive NO-$(NO)_2$ system using FF-a (green diamonds), the New FF (blue circles), and FF-b (red squares).

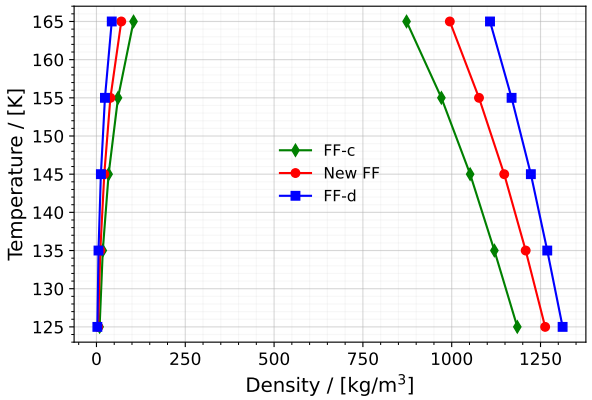

Figure S9: Orthobaric coexistence densities of the reactive NO-$(NO)_2$ system using FF-c (green diamonds), the New FF (blue circles), and FF-d (red squares).

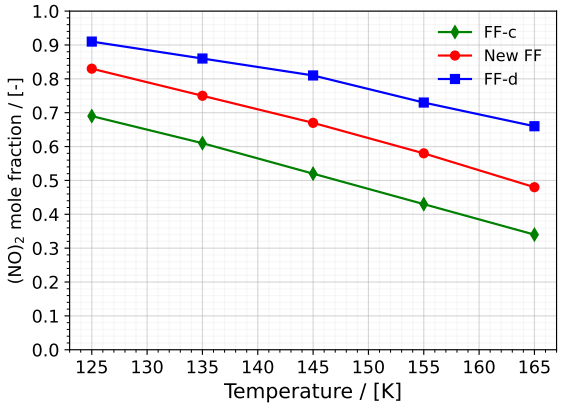

Figure S10: $(NO)_2$ mole fractions in the liquid phase of the reactive NO-$(NO)_2$ system using FF-c (green diamonds), the New FF (blue circles), and FF-d (red squares).

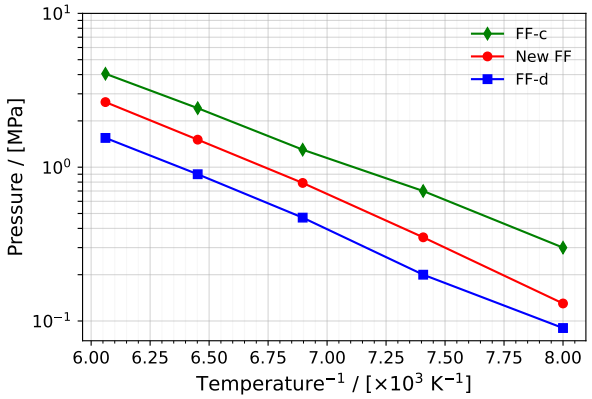

Figure S11: Inverse temperature dependence of the saturated vapor pressures of the reactive NO-$(NO)_2$ system using FF-c (green diamonds), the New FF (blue circles), and FF-d (red squares), in logarithmic scale.

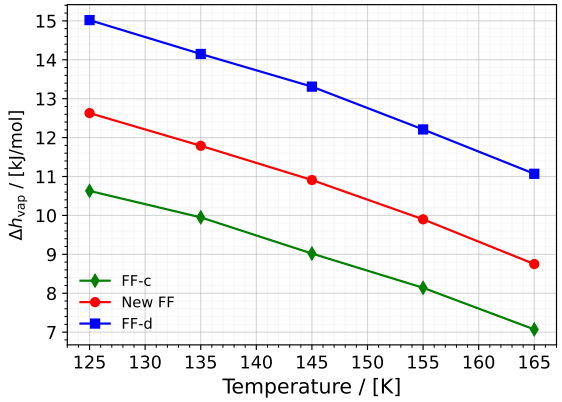

Figure S 12: Heats of vaporization of the reactive NO-$(NO)_2$ system using FF-c (green diamonds), the New FF (blue circles), and FF-d (red squares).

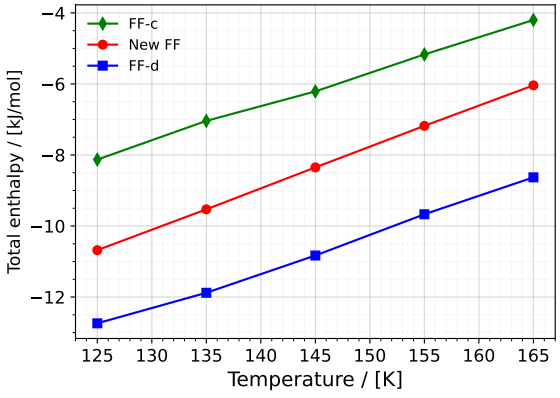

Figure S13: Total true molar enthalpies of the reactive NO-$(NO)_2$ system using FF-c (green diamonds), the New FF (blue circles), and FF-d (red squares).

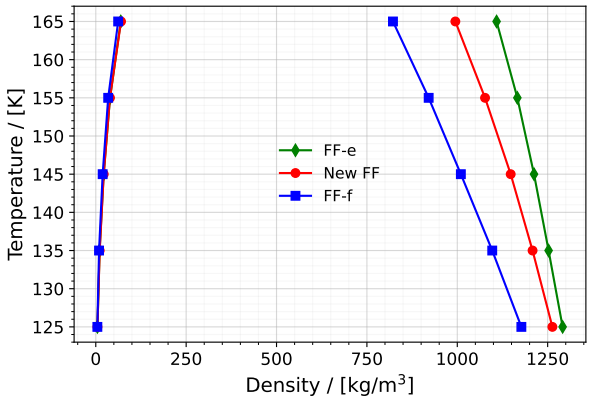

Figure S14: Orthobaric coexistence densities of the reactive NO-$(NO)_2$ system using FF-e (green diamonds), the New FF (blue circles), and FF-f (red squares).

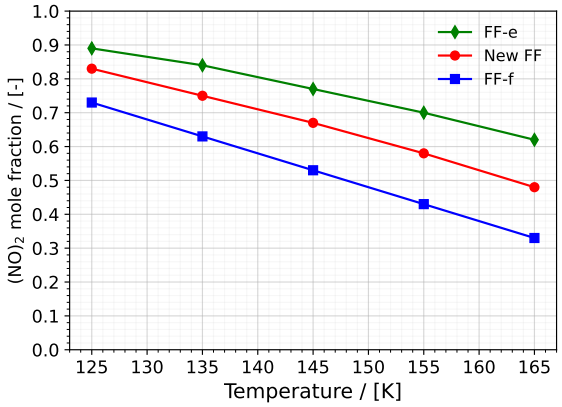

Figure S15: $(NO)_2$ mole fractions in the liquid phase of the reactive NO-$(NO)_2$ system using FF-e (green diamonds), the New FF (blue circles), and FF-f (red squares).

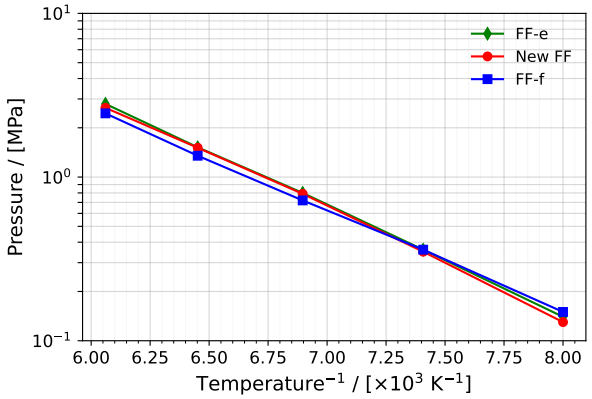

Figure S16: Inverse temperature dependence of the saturated vapor pressures of the reactive NO-$(NO)_2$ system using FF-e (green diamonds), the New FF (blue circles), and FF-f (red squares), in logarithmic scale.

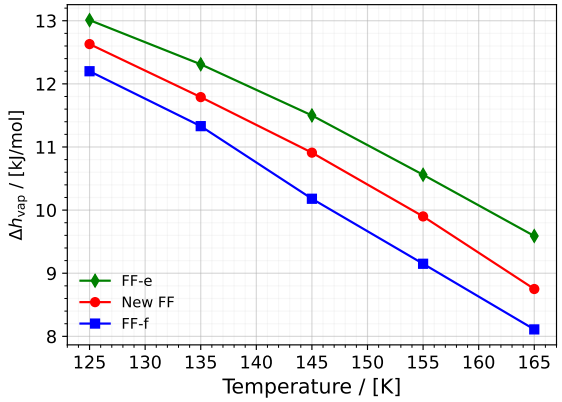

Figure S17: Heats of vaporization of the reactive NO-$(NO)_2$ system using FF-e (green diamonds), the New FF (blue circles), and FF-f (red squares).

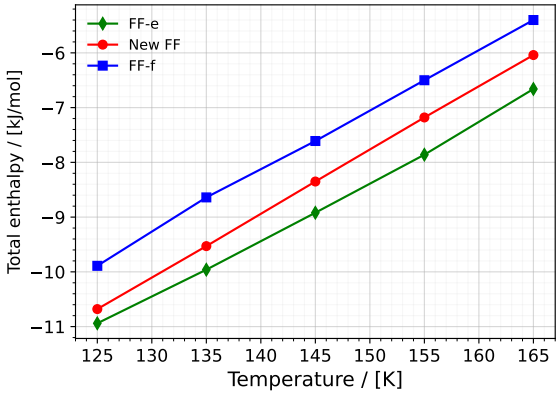

Figure S18: Total true molar enthalpies of the reactive NO-$(NO)_2$ system using FF-e (green diamonds), the New FF (blue circles), and FF-f (red squares).

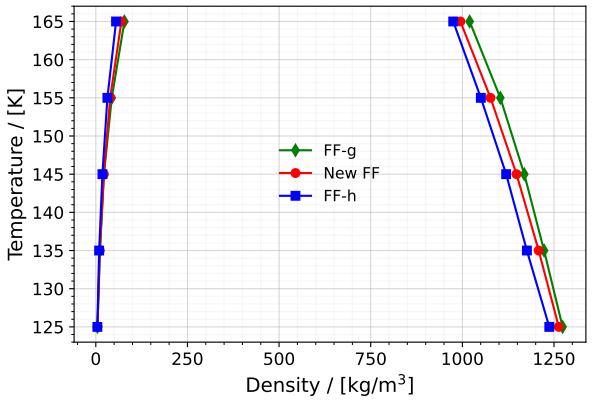

Figure S19: Orthobaric coexistence densities of the reactive NO-$(NO)_2$ system using FF-g (green diamonds), the New FF (blue circles), and FF-h (red squares).

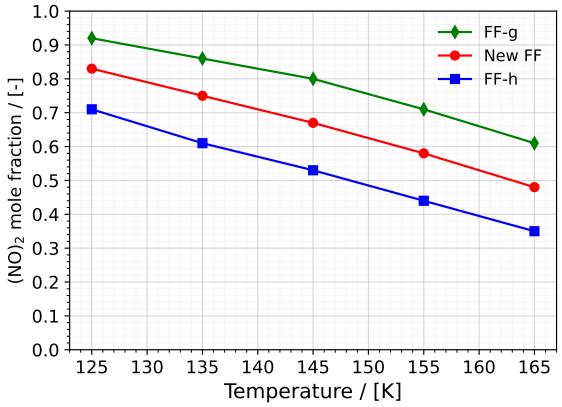

Figure S20: $(NO)_2$ mole fractions in the liquid phase of the reactive NO-$(NO)_2$ system using FF-g (green diamonds), the New FF (blue circles), and FF-h (red squares).

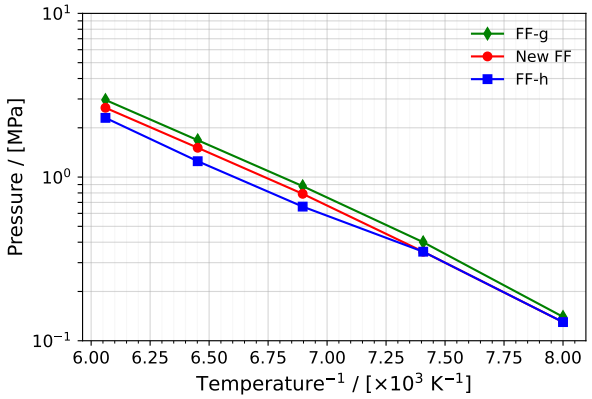

Figure S21: Inverse temperature dependence of the saturated vapor pressures of the reactive NO-$(NO)_2$ system using FF-g (green diamonds), the New FF (blue circles), and FF-h (red squares), in logarithmic scale.

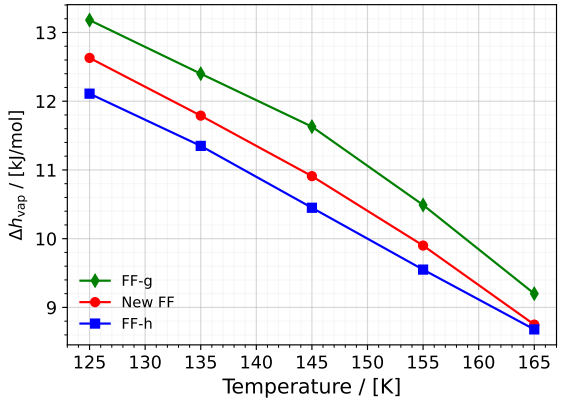

Figure S 22: Heats of vaporization of the reactive NO-$(NO)_2$ system using FF-g (green diamonds), the New FF (blue circles), and FF-h (red squares).

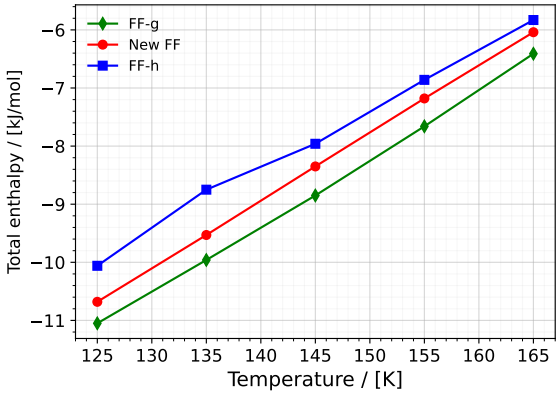

Figure S23: Total true molar enthalpies of the reactive NO-$(NO)_2$ system using FF-g (green diamonds), the New FF (blue circles), and FF-h (red squares).

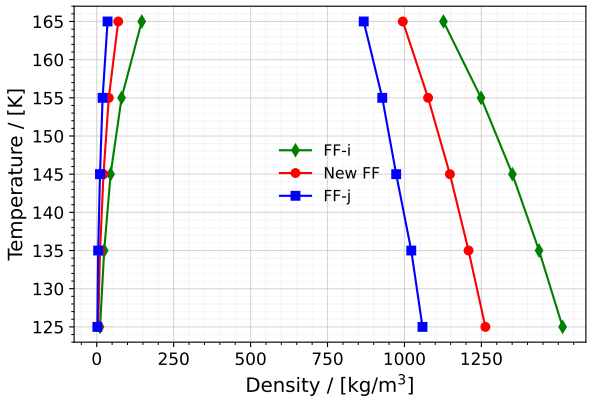

Figure S24: Orthobaric coexistence densities of the reactive NO-$(NO)_2$ system using FF-i (green diamonds), the New FF (blue circles), and FF-j (red squares).

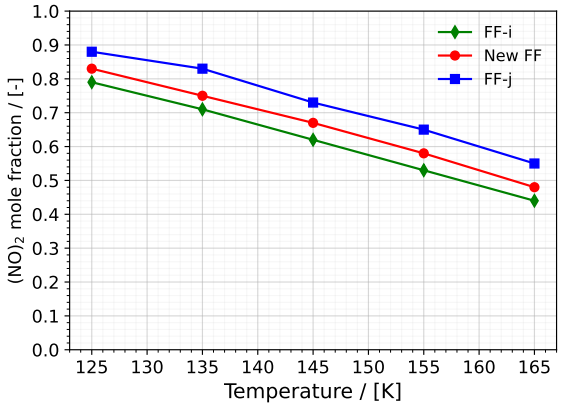

Figure S25: $(NO)_2$ mole fractions in the liquid phase of the reactive NO-$(NO)_2$ system using FF-i (green diamonds), the New FF (blue circles), and FF-j (red squares).

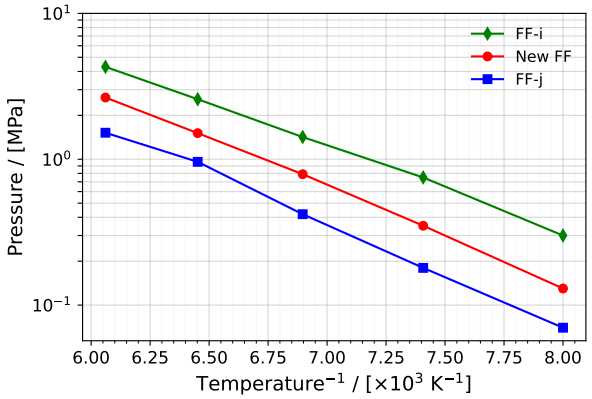

Figure S26: Inverse temperature dependence of the saturated vapor pressures of the reactive NO-$(NO)_2$ system using FF-i (green diamonds), the New FF (blue circles), and FF-j (red squares), in logarithmic scale.

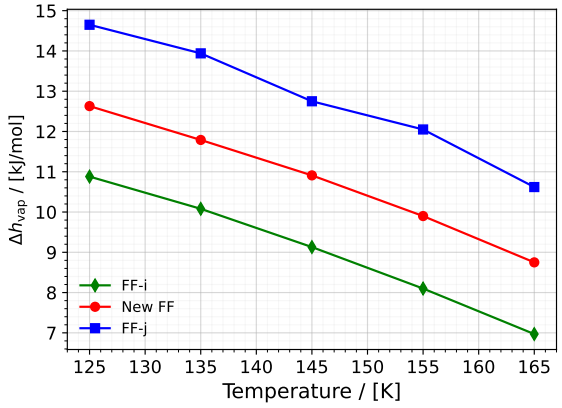

Figure S 27: Heats of vaporization of the reactive NO-$(NO)_2$ system using FF-i (green diamonds), the New FF (blue circles), and FF-j (red squares).

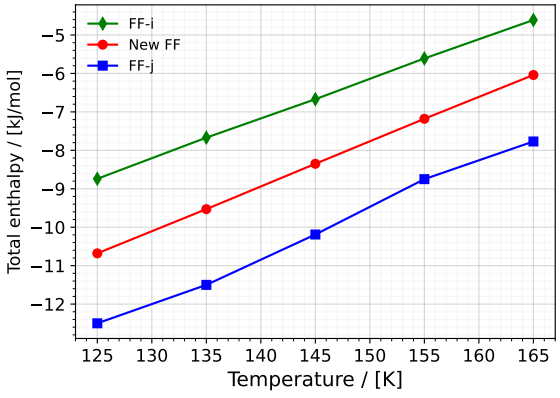

Figure S28: Total true molar enthalpies of the reactive NO-$(NO)_2$ system using FF-i (green diamonds), the New FF (blue circles), and FF-j (red squares).

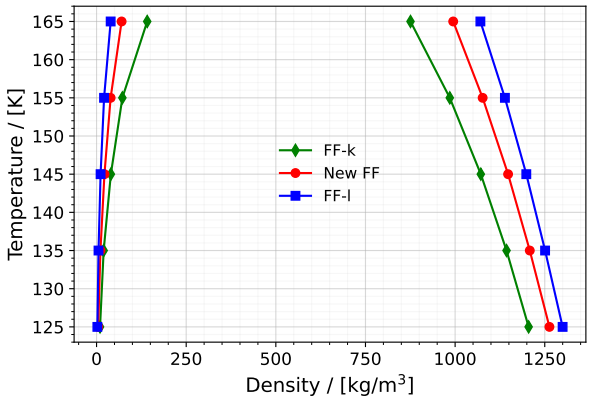

Figure S29: Orthobaric coexistence densities of the reactive NO-$(NO)_2$ system using FF-k (green diamonds), the New FF (blue circles), and FF-l (red squares).

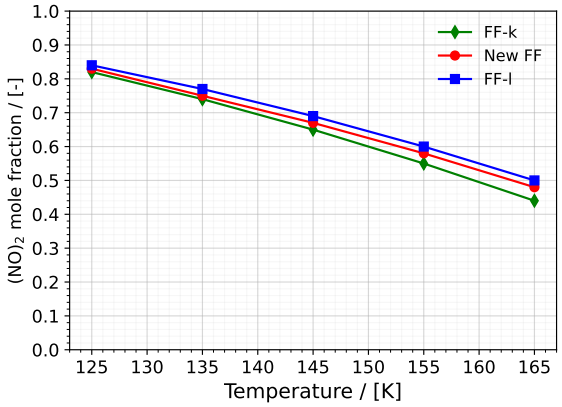

Figure S30: $(NO)_2$ mole fractions in the liquid phase of the reactive NO-$(NO)_2$ system using FF-k (green diamonds), the New FF (blue circles), and FF-l (red squares).

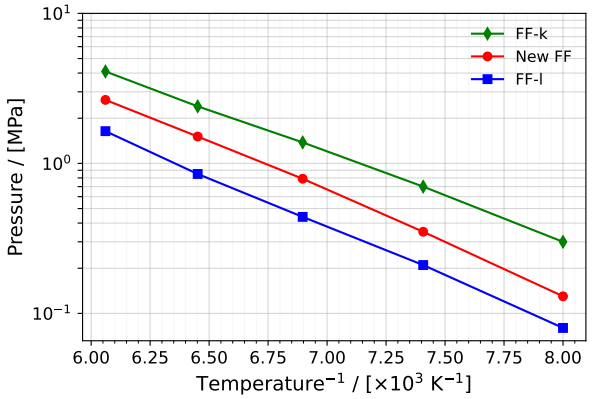

Figure S31: Inverse temperature dependence of the saturated vapor pressures of the reactive NO-$(NO)_2$ system using FF-k (green diamonds), the New FF (blue circles), and FF-l (red squares), in logarithmic scale.

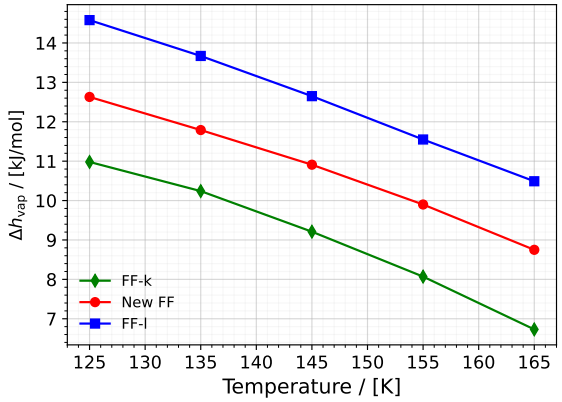

Figure S32: Heats of vaporization of the reactive NO-$(NO)_2$ system using FF-k (green diamonds), the New FF (blue circles), and FF-l (red squares).

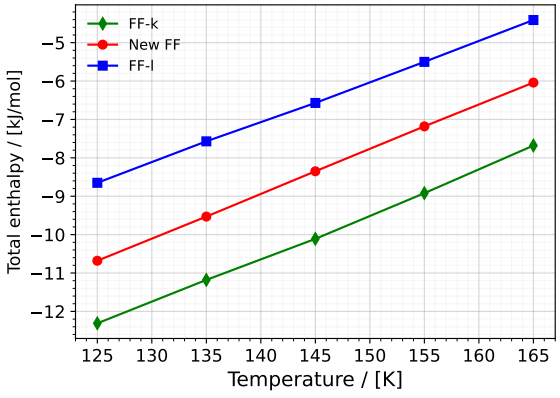

Figure S33: Total true molar enthalpies of the reactive NO-$(NO)_2$ system using FF-k (green diamonds), the New FF (blue circles), and FF-l (red squares).

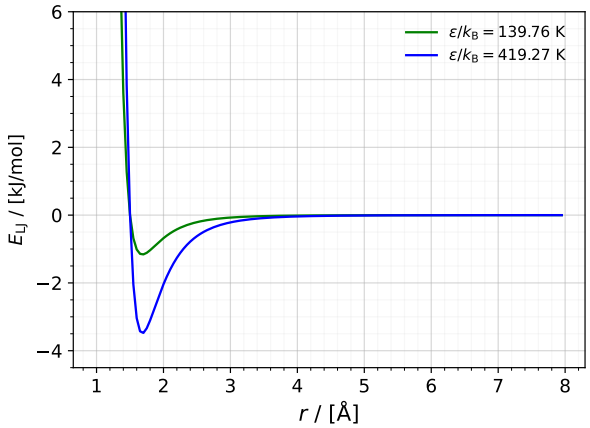

Figure S34: Lennard-Jones potential energy for two single-bead particles with different values of ϵ/k_B (139.76 K and 419.27 K) and identical value of σ (1.5 Å).

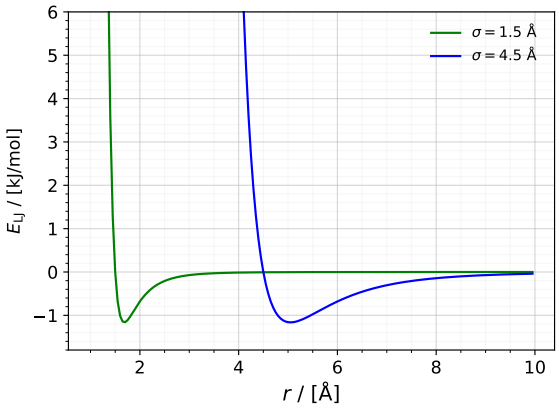

Figure S35: Lennard-Jones potential energy for two single-bead particles with different values of σ (1.5 Å and 4.5 Å) and identical value of ϵ/k_B (139.76 K).

References

(1) Horn, E. F.; Dickey, F. P. Near-Infrared Emission Spectrum of NO. *Journal of Chemical Physics* **1964**, *41*, 1614–1620.

(2) McKellar, A. R.; Watson, J.; Howard, B. The NO dimer: 15N isotopic infrared spectra, line-widths, and force field. *Molecular Physics* **1995**, *86*, 273–286.

(3) East, A.; McKellar, A.; Watson, J. The intermolecular vibrations of the NO dimer. *Journal of Chemical Physics* **1998**, *109*, 4378–4383.

(4) Glendening, E. D.; Halpern, A. M. Ab initio calculations of nitrogen oxide reactions: Formation of N_2O_2, N_2O_3, N_2O_4, N_2O_5, and N_4O_2, from NO, NO_2, NO_3, and N_2O. *Journal of Chemical Physics* **2007**, *127*, 164307–11.

(5) Western, C. M.; Langridge-Smith, P. R.; Howard, B. J.; Novick, S. E. Molecular beam electric resonance spectroscopy of the nitric oxide dimer. *Molecular Physics* **1981**, *44*, 145–160.

(6) Rowley, R.; Wilding, W.; Oscarson, J.; Zundel, N.; Marshall, T.; Daubert, T.; Danner, R. *DIPPR Data Compilation of Pure Chemical Properties*; AIChE, 2010.

(7) Smith, A. L.; Johnston, H. L. The magnetic susceptibility of liquid nitric oxide and the heat of dissociation of $(NO)_2$[1]. *Journal of the American Chemical Society* **1952**, *74*, 4696–4698.

(8) Walsh, J. M.; Guedes, H. J.; Gubbins, K. E. Physical theory for fluids of small associating molecules. *Journal of Physical Chemistry* **1992**, *96*, 10995–11004.

(9) Turner, C. H.; Johnson, J. K.; Gubbins, K. E. Effect of confinement on chemical reaction equilibria: The reactions $2NO \leftrightarrow (NO)_2$ and $N_2 + 3H_2 \leftrightarrow 2NH_3$ in carbon micropores. *Journal of Chemical Physics* **2001**, *114*, 1851–1859.

(10) Rohatgi, A. Webplotdigitizer: Version 4.5. *URL https://automeris.io/WebPlotDigitizer* **2020**, *411*.

(11) Zhou, Z.; Todd, B.; Travis, K. P.; Sadus, R. J. A molecular dynamics study of nitric oxide in water: diffusion and structure. *Journal of Chemical Physics* **2005**, *123*, 054505.

(12) Lachet, V.; Creton, B.; de Bruin, T.; Bourasseau, E.; Desbiens, N.; Wilhelmsen, Ø.; Hammer, M. Equilibrium and transport properties of CO_2+ N_2O and CO_2+ NO mixtures: Molecular simulation and equation of state modelling study. *Fluid Phase Equilibria* **2012**, *322*, 66–78.